

# Magnetic order in $\text{BaFe}_2\text{As}_2$ , the parent compound of the FeAs based superconductors in a new structural family

Q. Huang<sup>1</sup>, Y. Qiu<sup>1,2</sup>, Wei Bao<sup>3</sup>, J.W. Lynn<sup>1</sup>, M.A. Green<sup>1,2</sup>, Y.C. Gasparovic<sup>1,2</sup>, T. Wu<sup>4</sup>, G. Wu<sup>4</sup>  
& X. H. Chen<sup>4</sup>

<sup>1</sup>*NIST Center for Neutron Research, National Institute of Standards and Technology, Gaithersburg, MD 20899, USA*

<sup>2</sup>*Department of Materials Science and Engineering, University of Maryland, College Park, MD 20742, USA*

<sup>3</sup>*Los Alamos National Laboratory, Los Alamos, NM 87545, USA*

<sup>4</sup>*Hefei National Laboratory for Physical Science at Microscale and Department of Physics, University of Science and Technology of China, Hefei, Anhui 230026, China*

**In addition to higher superconducting transition temperatures ( $T_C \sim 55$  K) compared with the ubiquitous cuprates for materials composed of a single electronically active layer<sup>1-4</sup>, the newly discovered iron oxypnictide superconductors offer additional compositional variation. The family of FeAs based superconductors with the same ZrCuSiAs-type (1111-type) structure now include  $Ln\text{FeAsO}$ ,  $Ln=\text{La, Sm, Ce, Nd, Pr, Gd, Tb or Dy}$ <sup>1-12</sup>. In a similar fashion to the corner shared  $\text{CuO}_2$  layers present in cuprates, the FeAs layers, now formed by edge-shared  $\text{FeAs}_4$  tetrahedra, dominate the electronic states that produce superconductivity<sup>13-15</sup>. Cuprate superconductors distinguish themselves structurally by adopting different stacking sequences of the Cu-O and electronically inactive “spacer” layers. Using the same structural**

philosophy, layered materials with the formula  $(A,K)Fe_2As_2$ ,  $A=Ba$  or  $Sr$ , which crystallize in a different  $ThCr_2Si_2$ -type (122-type) structure, have recently been reported and possess a  $T_C$  as high as 38 K<sup>16-19</sup>. Here, we report the neutron diffraction studies of  $BaFe_2As_2$  that show, in contrast to previous studies on the 1111-type materials<sup>20-23</sup>, a phase transition to a long-ranged antiferromagnetic state at a temperature where a structural transition from tetragonal to orthorhombic symmetry also occurs. The discontinuity in the intensity of the  $(220)_T$  Bragg reflection implies a first-order transition as a result of the greater flexibility within the nonequivalent layers. This is in contrast to the second-order transition seen for the previously reported 1111-type materials<sup>20-23</sup>. Although the magnetic and structural transitions occur differently in the  $BaFe_2As_2$  and the 1111-type materials, this work clearly demonstrates that the complete evolution to a low symmetry structure is a pre-requirement for the iron magnetic order to occur.

Like the parent compounds  $LnFeAsO$  of the 1111-type FeAs superconductors, the 122-type parent compounds  $BaFe_2As_2$  and  $SrFe_2As_2$  are not superconducting and show a similar pronounced anomaly in resistivity at  $T_S \sim 140$  K<sup>16,19,24</sup> and 205 K<sup>17,18,25</sup>, respectively. Structural refinements have been performed only for  $BaFe_2As_2$  using X-ray powder diffraction, and a second-order structural phase-transition at  $T_S$  has been concluded to cause the resistivity anomaly like in  $LaFeAsO$ <sup>24</sup>. The <sup>57</sup>Fe Mössbauer spectra have been measured at 298, 77 and 4.2 K for  $BaFe_2As_2$ , and long-range magnetic order exists at 77 and 4.2 K<sup>24</sup>. No such spectroscopic studies have yet been performed for  $SrFe_2As_2$ . Careful specific heat measurements, however, indicate the phase transition at  $T_S \approx 205$  K in  $SrFe_2As_2$  as a first-order one<sup>25</sup>. So far, no magnetic structure

in the new 122-type materials has been reported, neither is it clear whether the magnetic transition concurs with the structural transition at  $T_S$  or is a separate phase transition as in  $\text{LaFeAsO}^{20,21}$  or  $\text{NdFeAsO}^{22,23}$ .

We synthesized 2 g of polycrystalline  $\text{BaFe}_2\text{As}_2$  sample using the solid state reaction as described in Ref. [19]. The resistivity was measured using the standard four-probe method while the sample was cooled. As shown in Fig. 1, the drop of resistivity at  $T_S \approx 142$  K is sudden and steep, as reported by Krellner et al. for  $\text{SrFe}_2\text{As}_2$ <sup>25</sup>. Neutron powder diffraction spectra were measured with neutrons of wavelength  $\lambda = 2.079\text{\AA}$ , using the high resolution powder diffractometer BT1 at the NIST Center for Neutron Research (NCNR). The sample temperature was controlled by a closed cycle refrigerator. The spectrum measured at 175 K is shown in Fig. 2(a) together with the refined profile obtained with the GSAS program<sup>26</sup>. Consistent with previous studies<sup>24</sup>, the high temperature structure is well accounted for by the tetragonal  $\text{ThCr}_2\text{Si}_2$ -type structure, and the structural parameters from the refinement using space group  $I4/mmm$  are listed in Table 1(a).

The neutron powder diffraction spectrum measured at 5 K is shown in Fig. 2(b). Our neutron data confirm the orthorhombic structural distortion previously reported in the X-ray study<sup>24</sup>, which splits the  $(220)_T$  Bragg peak of the  $I4/mmm$  tetragonal unit cell, shown in the inset to Fig. 2(a), into two Bragg peaks  $(400)_O$  and  $(040)_O$  of the  $Fmmm$  orthorhombic unit cell as marked in Fig. 2(b). To clarify the nature of the structural transition at  $T_S \approx 142$  K, we followed the diffraction intensity at  $2\theta = 95.8^\circ$  as a function of temperature. Above  $T_S$ , this angle corresponds to the peak position of the  $(220)_T$ ; below  $T_S$ , it corresponds to the valley between the  $(400)_O$  and

(040)<sub>O</sub> peaks, see inset to Fig. 1. The intensity changes in an abrupt first-order fashion as shown in Fig. 1. Additionally, hysteresis was observed during a cooling and warming cycle with a temperature change rate of 15 K/h. Therefore, while the pronounced anomaly in resistivity is associated with the tetragonal-to-orthorhombic structural transition in both the 122 and 1111-types of the FeAs based materials, the structural transition in the newer 122-type material to a low symmetry structure occurs over a much reduced temperature range, implying a transition first order in nature.

Additional magnetic Bragg peaks are apparent in the neutron diffraction patterns measured below  $T_S$ . In the inset to Fig. 2(b), magnetic Bragg peaks from the 5K spectrum are highlighted by the vertical lines and are indexed using the orthorhombic unit cell. Irreducible representational analysis for BaFe<sub>2</sub>As<sub>2</sub> in the  $Fmmm$  space group shows magnetic moments are allowed along all three axis. Furthermore, the first order nature of the transition allows for any combination of these moments to contribute to the overall magnetic structure. Analysis of the magnetic Bragg reflections reveals a simple antiferromagnetic structure within the eight Fe ions in the orthorhombic unit cell. The magnetic and crystal parameters determined in a combined structural and magnetic refinement of the 5 K spectrum in Fig. 2(b) are listed in Table 1(b), and the magnetic structure of BaFe<sub>2</sub>As<sub>2</sub> is depicted in Fig. 3. It should be noted that although the magnetic structure is depicted along one axis, this is a representational solution and indistinguishable by our powder neutron data from other models where the moments lie in the ab plane. As the FeAs layers are identical in this 122 structure to LaFeAsO, it is unsurprising that the magnetic structure within the FeAs layer of BaFe<sub>2</sub>As<sub>2</sub> is also identical<sup>20</sup>. This demonstrates a commonality of the magnetic interactions within the Fe layers and variation in the stacking of the layers, and therefore the interactions along the c

axis, do not contribute greatly to the overall magnetic structure.

The ordered magnetic moment  $0.87(3) \mu_B$  per Fe at 5 K in  $\text{BaFe}_2\text{As}_2$ , however, is substantially larger than the saturated moment  $0.36(5) \mu_B$  per Fe in  $\text{LaFeAsO}^{20}$ , but is comparable to the iron moment  $0.9(1) \mu_B$  in  $\text{NdFeAsO}$  which possesses a different antiferromagnetic structure<sup>23</sup>.  $\text{BaFe}_2\text{As}_2$  differs most significantly from  $\text{LaFeAsO}$  in that the antiferromagnetic transition occurs at a temperature that is indistinguishable from the structural transition, in contrast to all previously measured FeAs based 1111-type materials where both the high and low temperature structures co-exist over a wide temperature range<sup>20-23</sup>. Fig. 4 shows the temperature dependence of the magnetic Bragg peak  $(101)_M$ , measured at the higher flux triple-axis spectrometer BT7 at NCNR. The solid line represents the mean-field theoretical fit for the squared magnetic order parameter and the Néel temperature is determined at  $T_N = 143(4)$  K, which is the same value determined for the structural transition. It is clear from these measurements, that the important criteria for the onset of magnetic order is the complete disappearance of the high temperature phase. The additional flexibility afforded in the 122-type structure by the nearest neighbour layers being displaced by  $(a/2, b/2)$  from each other clearly allows the structural strain to be relieved over a shorter temperature range than allowed for the single layered 1111-type systems.

Soon after the discovery of the  $\text{LaFeAs}(\text{O},\text{F})$  superconductor<sup>5</sup>, it was recognized that there exist nesting Fermi surfaces connected by the wave vector  $(1/2, 1/2, 0)_T$  in the calculated electronic band structures of the parent compound  $\text{LaFeAsO}^{27-29}$ , and the resistivity anomaly of  $\text{LaFeAsO}$  at  $\sim 150$  K was predicted to be caused by the resulting spin-density-wave (SDW) order<sup>30</sup>. Since

the electronic states near the Fermi surfaces come predominantly from the five  $d$ -orbitals of the Fe ions<sup>13-15</sup>, the SDW represents an antiferromagnetic order of Fe. It turns out that the anomaly is instead associated with a structural transition, and the antiferromagnetic transition was observed at  $\sim 137$  K in a separated phase-transition<sup>20</sup>. Additionally, the observed magnetic moment of the Fe ion is an order of magnitude weaker than the theoretically predicated  $\sim 2.3 \mu_B$  per Fe<sup>28,29</sup>. Frustrating magnetic exchange interactions have been invoked to explain the small observed moment in LaFeAsO<sup>31,32</sup>. In another 1111-type material, NdFeAsO, for which magnetic structure has been determined, magnetic transition was observed only at 1.96 K in a combined Nd and Fe antiferromagnetic order, in spite of the fact that the resistivity anomaly and the structural transition concur at  $\sim 150$  K<sup>23</sup>. No separated Fe order at elevated temperatures has been observed yet. While the predication of the resistivity anomaly caused by the SDW transition has not been realized for the intended 1111-type materials, it is not clear whether its occurrence in BaFe<sub>2</sub>As<sub>2</sub> is fortuitous since no theoretical work on the new 122-type materials has been reported. The antiferromagnetic spin fluctuations characterized by the SDW wavevector (1/2,1/2,0) have been invoked in a large number of theoretical works as the bosonic mode to mediate the Cooper pairs in the FeAs-based new high  $T_C$  superconductors. Before these theories gain acceptance, the general aspects of the magnetism of these materials need to be firmly established and satisfactorily explained.

1. Ren, Z. A. *et al.* Superconductivity at 55 K in iron-based F-doped layered quaternary compound Sm[O<sub>1-x</sub>F<sub>x</sub>]FeAs. *Chinese Phys. Lett.* **25**, 2215 (2008).
2. Liu, R. H. *et al.* Phase Diagram and Quantum Critical Point in Newly Discovered Supercon-

- ductors:  $\text{SmO}_{1-x}\text{F}_x\text{FeAs}$ . *arXiv:0804.2105* (2008).
3. Ren, Z.-A. *et al.* Superconductivity and Phase Diagram in Iron-based Arsenic-oxides  $\text{ReFeAsO}_{1-\delta}$  without Fluorine Doping. *arXiv:0804.2582* (2008).
  4. Wang, C. *et al.* Thorium-doping induced superconductivity in  $\text{Gd}_{1-x}\text{Th}_x\text{OFeAs}$ . *arXiv:0804.4290* (2008).
  5. Kamihara, Y., Watanabe, T., Hirano, M. & Hosono, H. Iron-Based Layered Superconductor  $\text{La}[\text{O}_{1-x}\text{F}_x]\text{FeAs}$  ( $x=0.05 - 0.12$ ) with  $T_c=26\text{K}$ . *J. Am. Chem. Soc.* **130**, 3296 (2008).
  6. Chen, X. H. *et al.* Superconductivity at 43 K in  $\text{SmFeAsO}_{1-x}\text{F}_x$ . *Nature* **453**, 761 (2008).
  7. Chen, G. F. *et al.* Superconductivity at 41 K and its competition with spin-density-wave instability in layered  $\text{CeO}_{1-x}\text{F}_x\text{FeAs}$ . *arXiv:0803.3790 (Phys. Rev. Lett. in press)* (2008).
  8. Ren, Z. A. *et al.* Superconductivity in iron-based F-doped layered quaternary compound  $\text{Nd}[\text{O}_{1-x}\text{F}_x]\text{FeAs}$ . *Europhys. Lett.* **82**, 57002 (2008).
  9. Ren, Z. A. *et al.* Superconductivity at 52 K in iron-based F-doped layered quaternary compound  $\text{Pr}[\text{O}_{1-x}\text{F}_x]\text{FeAs}$ . *arXiv:0803.4283* (2008).
  10. Chen, G. F. *et al.* Element substitution effect in transition metal oxypnictide  $\text{Re}(\text{O}_{1-x}\text{F}_x)\text{TAs}$  (Re=rare earth, T=transition metal). *Chinese Phys. Lett.* **25**, 2235 (2008).
  11. Ren, Z. A. *et al.* Superconductivity at 53.5 K in  $\text{GdFeAsO}_{1-\delta}$ . *Supercond. Sci. Technol.* **21**, 082001 (2008).

12. Bos, J.-W. G. *et al.* High pressure synthesis of late rare earth  $R\text{FeAs}(\text{O},\text{F})$  superconductors;  $R = \text{Tb}$  and  $\text{Dy}$ . *arXiv:0806.0926* (2008).
13. Singh, D. J. & Du, M.-H.  $\text{LaFeAsO}_{1-x}\text{F}_x$ : A low carrier density superconductor near itinerant magnetism. *arXiv:0803.0429 (Phys. Rev. Lett. in-press)* (2008).
14. Haule, K., Shim, J. H. & Kotliar, G. Correlated electronic structure of  $\text{LaFeAsO}_{1-x}\text{F}_x$ . *arXiv:0803.1279* (2008).
15. Xu, G. *et al.* Doping-dependent Phase Diagram of LaOMAs ( $\text{M}=\text{V-Cu}$ ) and Electron-type Superconductivity near Ferromagnetic Instability. *arXiv:0803.1282 (Europhys. Lett. in-press)* (2008).
16. Rotter, M., Tegel, M. & Johrendt, D. Superconductivity at 38 K in the iron arsenide  $(\text{Ba}_{1-x}\text{K}_x)\text{Fe}_2\text{As}_2$ . *arXiv:0805.4630* (2008).
17. Chen, G. F. *et al.* Superconductivity in hole-doped  $(\text{Sr}_{1-x}\text{K}_x)\text{Fe}_2\text{As}_2$ . *arXiv:0806.1209* (2008).
18. Sasmal, K. *et al.* Superconductivity up to 37 K in  $(\text{A}_{1-x}\text{Sr}_x)\text{Fe}_2\text{As}_2$  with  $\text{A} = \text{K}$  and  $\text{Cs}$ . *arXiv:0806.1301* (2008).
19. Wu, G. *et al.* Transport properties and superconductivity in  $\text{Ba}_{1-x}\text{M}_x\text{Fe}_2\text{As}_2$  ( $\text{M}=\text{La}$  and  $\text{K}$ ) with double FeAs layers. *arXiv:0806.1459* (2008).
20. Cruz, C. *et al.* Magnetic order close to superconductivity in the iron-based layered  $\text{La}(\text{O}_{1-x}\text{F}_x)\text{FeAs}$  systems. *Nature* **453**, 899 (2008).

21. Nomura, T. *et al.* Crystallographic Phase Transition and High-Tc Superconductivity in LaOFeAs:F. *arXiv:0804.3569* (2008).
22. Bos, J.-W. G. *et al.* Influence of the Nd<sup>3+</sup> Moments on the Magnetic Behaviour of the Oxypnictides superconductors NdFeAsO<sub>1-x</sub>F<sub>x</sub>. *arXiv:0806.1450* (2008).
23. Qiu, Y. *et al.* The absence of the spin-density-wave order in the NdFeAsO<sub>1-x</sub>F<sub>x</sub> high Tc superconductor system. *arXiv:0806.2195* (2008).
24. Rotter, M. *et al.* Spin density wave anomaly at 140 K in the ternary iron arsenide BaFe<sub>2</sub>As<sub>2</sub>. *arXiv:0805.4021* (2008).
25. Krellner, C. *et al.* Magnetic and structural transitions in layered FeAs systems: AFe<sub>2</sub>As<sub>2</sub> versus RFeAsO compounds. *arXiv:0806.1043* (2008).
26. A. Larson and R.B. Von Dreele, *GSAS: Generalized Structure Analysis System*, (Los Alamos National Laboratory, 1994).
27. Mazin, I. I., Singh, D. J., Johannes, M. D. & Du, M. H. Unconventional sign-reversing superconductivity in LaFeAsO<sub>1-x</sub>F<sub>x</sub>. *arXiv:0803.2740* (2008).
28. Cao, C., Hirschfeld, P. J. & Cheng, H. P. Coexistence of antiferromagnetism with superconductivity in LaFeAsO<sub>1-x</sub>F<sub>x</sub>: effective Hamiltonian from ab initio studies. *arXiv:0803.3236* (2008).
29. Ma, F. & Lu, Z. Y. Iron-based layered superconductor LaFeAsO<sub>1-x</sub>F<sub>x</sub>: an antiferromagnetic semimetal. *arXiv:0803.3286* (2008).

30. Dong, J. *et al.* Competing Orders and Spin-Density-Wave Instability in  $\text{La}(\text{O}_{1-x}\text{F}_x)\text{FeAs}$ . *arXiv:0803.3426 (Europhys. Lett. in-press)* (2008).
31. Yildirim, T. Origin of the 150 K Anomaly in  $\text{LaOFeAs}$ ; Competing Antiferromagnetic Superexchange Interactions, Frustration, and Structural Phase Transition. *arXiv:0804.2252* (2008).
32. Si, Q. & Abrahams, E. Strong Correlations and Magnetic Frustration in the High Tc Iron Pnictides. *arXiv:0804.2480* (2008).

**Acknowledgements** Work at LANL is supported by U.S. DOE, at USTC by the Natural Science Foundation of China, Ministry of Science and Technology of China (973 Project No: 2006CB601001) and by National Basic Research Program of China (2006CB922005).

**Author information** The authors declare that they have no competing financial interests. Correspondence and requests for materials should be addressed to W.B. (wbao@lanl.gov).

Table 1. Structure parameters for BaFe<sub>2</sub>As<sub>2</sub> at (a)175 K and (b) 5 K.

(a) Space group *I4/mmm* (No.139),  $a=3.95702$  (4) Å and  $c=12.9685$  (2) Å.

Atom	site	$x$	$y$	$z$	$B(\text{Å}^2)$
Ba	$2a$	0	0	0	0.53(5)
Fe	$4d$	1/2	0	1/4	0.72(2)
As	$4e$	0	0	0.35405(8)	0.80(3)

$R_p=4.71\%$ ,  $wR_p=6.06\%$ ,  $\chi^2=1.109$

(b) Space group *Fmmm* (No.69),  $a=5.61587$ (5) Å,  $b=5.57125$ (5) Å,  $c=12.9428$ (1) Å.

Atom	Site	$x$	$y$	$z$	$B(\text{Å}^2)$	$Mx$ ( $\mu_B$ )
Ba	$4a$	0	0	0	0.20(4)	
Fe	$8f$	1/4	1/4	1/4	0.35(2)	0.87(3)
As	$8i$	0	0	0.35406(7)	0.47(3)	

$R_p=3.61\%$ ,  $wR_p=4.58\%$ ,  $\chi^2=1.825$ .

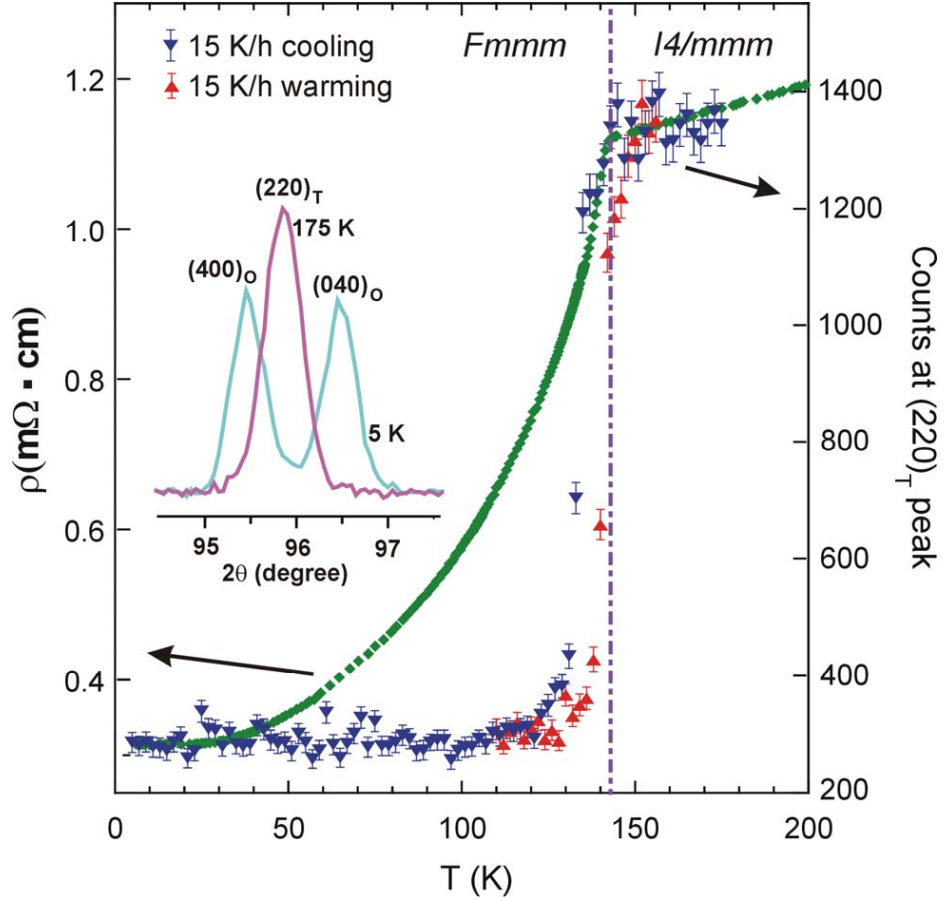


Figure 1 The resistivity of  $\text{BaFe}_2\text{As}_2$  as a function of temperature, measured while cooling, shows a sharp drop at  $T_S \approx 142$  K. The resistivity anomaly is associated with a first-order structural transition, as indicated by the neutron diffraction intensity at diffraction angle  $2\theta = 95.8^\circ$ . Inset: Neutron diffraction spectra measured above and below the structural transition, showing the splitting of the peak below  $T_S$ .

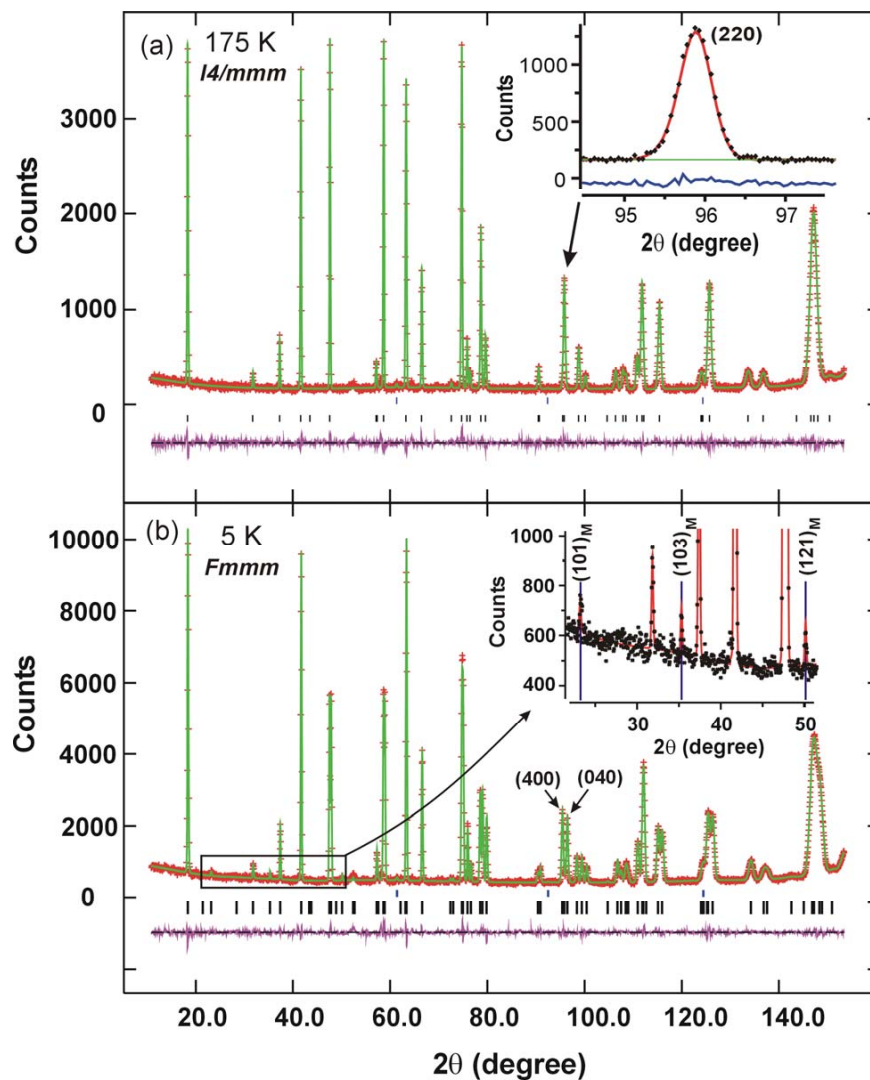


Figure 2 Neutron powder diffraction spectra at (a) 175 and (b) 5 K. The high temperature spectrum is refined with the tetragonal  $I4/mmm$  space group; the low temperature one with the orthorhombic  $Fmmm$  space group together with the magnetic structure shown in Fig. 3. The (220) Bragg peak in (a) is split into the (400) and (040) in (b) by the orthorhombic structural distortion.

Magnetic peaks at 5 K are highlighted in the inset to (b).

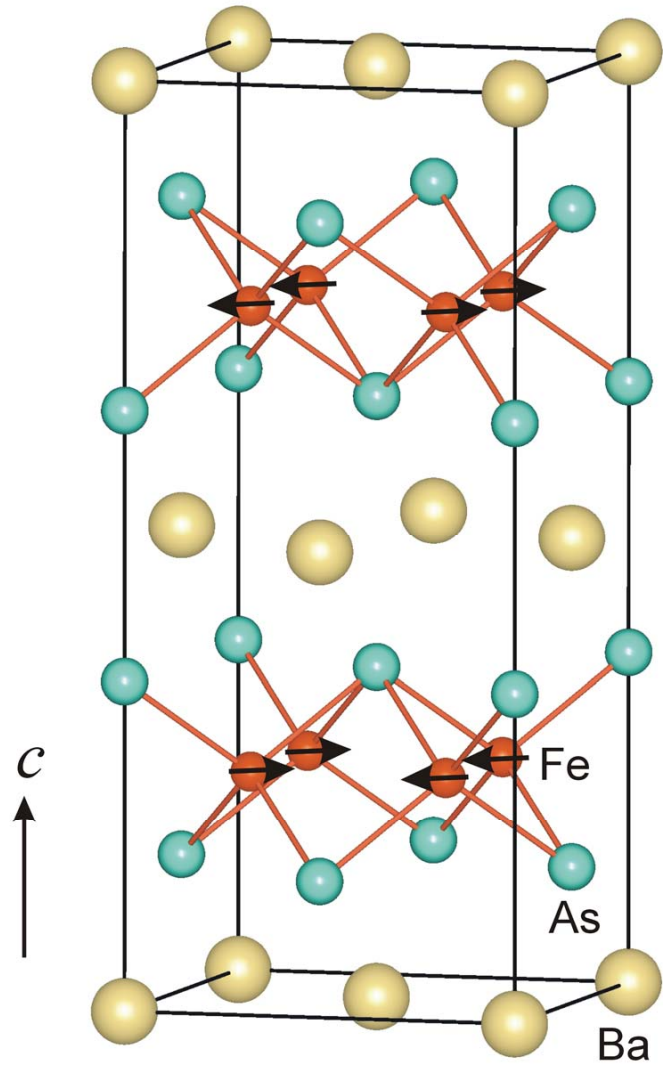


Figure 3 Magnetic and crystal structures of BaFe<sub>2</sub>As<sub>2</sub> shown in an orthorhombic *Fmmm* unit cell.

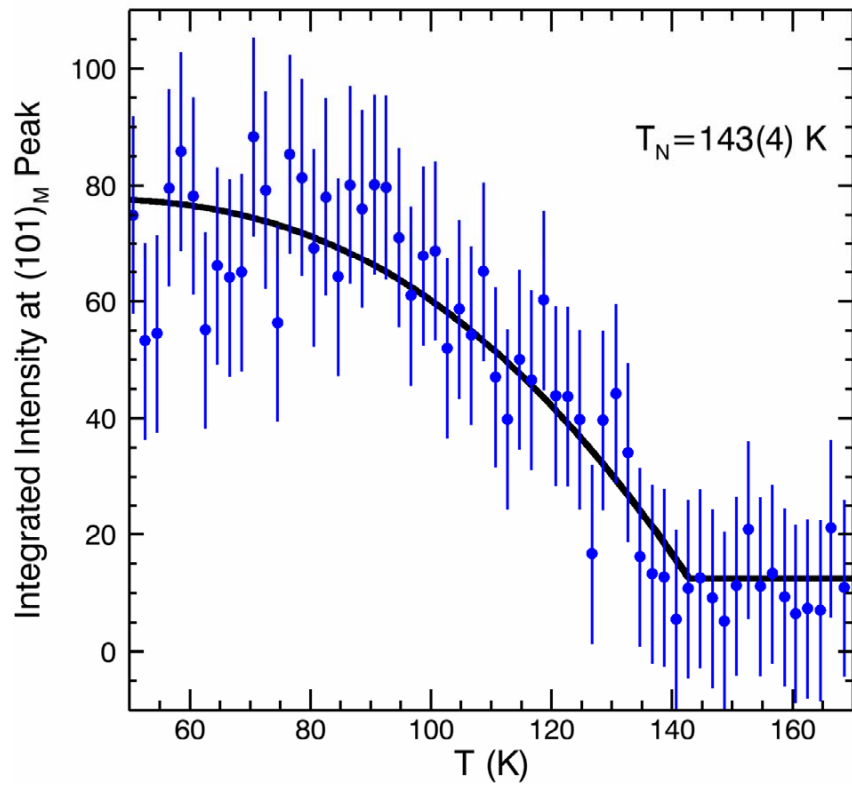


Figure 4 Magnetic Bragg peak  $(101)_M$  as a function of temperature. The solid line represents the least-square fit to mean-field theory for the squared order-parameter.